Materials and Structures (2009) 42:1353–1367
DOI 10.1617/s11527-008-9454-y

ORIGINAL ARTICLE

A numerical approach to modelling size effects on the flexural ductility of RC beams

A. Carpinteri · M. Corrado · G. Mancini · M. Paggi

Received: 22 April 2008 / Accepted: 24 November 2008 / Published online: 6 December 2008

Abstract The problem of evaluating the rotation capacity of reinforced concrete (RC) beams in bending has been largely investigated from both the experimental and the analytical point of view during the last decades. Since the development of ductility is influenced by several design parameters, it is difficult to develop a predictive model that can fully describe the mechanical behaviour of RC beams. In particular, the role of the size-scale effect, which has been evidenced by some experimental tests, is not yet completely understood. One of the main reasons is the inadequacy of the traditional models based on ad hoc stress–strain constitutive laws. In the present paper, a new model based on the concept of strain localization is proposed, which is able to describe both cracking and crushing growths in RC beams during the loading process. In particular, the nonlinear behaviour of concrete in compression is modelled by the *Overlapping Crack Model*, which describes the strain localization due to crushing by means of a material interpenetration. With this algorithm in hand, it is possible to effectively capture the flexural behaviour of RC beams by varying the reinforcement percentage and/or the beam depth. An extensive comparison with experimental results demonstrates the effectiveness of the proposed approach.

Keywords Plastic rotation · Ductility · Overlapping Crack Model · Crushing · Cohesive Crack Model · Size-scale effects · Reinforced concrete · Nonlinear analysis

1 Introduction

The development of considerable ductility in the ultimate limit state is a key parameter for the design of reinforced concrete (RC) beams in bending [1–5]. The interest in ductility was formerly connected with the diffusion of plastic analysis in the design of reinforced concrete structures [2, 6, 7]. In this context, in fact, the rotational capacity is required to allow the bending moment redistribution in statically indeterminate structures. Besides, the ductility contributes to satisfy many other requirements, absolutely necessary in order to guarantee the structural safety, as, e.g., to provide robustness, to give warning of incipient collapse by the development of large deformation prior to collapse and to enable major distortions and energy dissipation during earthquakes. The ductility can be suitably evaluated by means of the plastic rotation. With this aim in view two possible definitions of plastic rotation have been proposed. In accordance with the Model Code

A. Carpinteri · M. Corrado (✉) · G. Mancini · M. Paggi
Department of Structural Engineering and Geotechnics, Politecnico di Torino, Corso Duca degli Abruzzi 24, 10129 Torino, Italy
e-mail: mauro.corrado@polito.it

90 [8], such a rotation is defined as the difference between the rotation corresponding to the maximum resisting moment and the rotation corresponding to steel yielding, as schematically represented by $\vartheta_{PL}^{(1)}$ in Fig. 1. In order to take into account the development of ductility beyond the maximum resisting moment, Hillerborg [9] and Pecce and Fabbrocino [10] proposed an alternative measure of the plastic rotation, defined as the difference between the rotation beyond which the moment starts descending sharply and the rotation corresponding to steel yielding, see $\vartheta_{PL}^{(2)}$ in Fig. 1. Both measures increase by increasing the ductility of RC beams.

Due to its importance to guarantee structural safety, the rotation capacity of RC beams was largely studied from an experimental point of view since 1950s. Several experimental programmes permitted to highlight which are the main parameters influencing the development of plastic hinges: the steel ductility [11–14], the presence of the shear action in the hinge region [15–19], the concrete compression strength [10, 20, 21], the reinforcement in the compression zone [22], the confinement of concrete by means of stirrups [20, 22, 23], as well as the structural dimension [24–27].

The analytical assessment of the available ductility is difficult to be achieved due to the simultaneous presence of different nonlinear contributions: cohesive crack opening in tension, concrete crushing in compression and steel yielding or slippage. On the other hand, oversimplifications, based on the hypotheses usually assumed for the evaluation of the structural resistance, as, e.g., to neglect the concrete contribution in tension and to describe the nonlinear behaviour of concrete in compression and steel in tension by means of $\sigma - \varepsilon$ constitutive laws, does not permit to model all the experimentally observed effects on the ductility of RC beams in bending. In particular, it is impossible to catch the size-scale effects, because the aforementioned constitutive laws consider only an energy dissipation within the volume in the nonlinear regime.

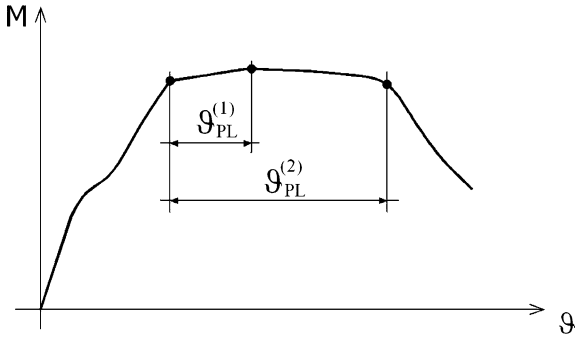

Fig. 1 Definitions of plastic rotation

The first fundamental contribution to the analytical assessment of the available ductility comes from the research carried out in the early 1980s at the University of Stuttgart by the Group coordinated by Eligehausen [11, 17]. The model developed by this Group, based on the description of the bond-slip behaviour between concrete and steel, is able to capture the structural behaviour by varying the ductility parameters of steel. Further improvement for the analysis of the behaviour of RC beams in bending was marked by the pioneering paper by Hillerborg in 1990 [9], who introduced the concept of strain localization in concrete in compression. According to his approach, when the ultimate compression strength is achieved, a strain localization takes place within a characteristic length proportional to the depth of the compressed zone. This model permits to address the issue of size effects, although the definition of the length over which the strain localization occurs is a free parameter and its value is not defined on the basis of theoretical arguments. Afterwards, several models have been developed on the basis of the Stuttgart and the Hillerborg proposals, emphasizing some more specific aspects [28–31]. In spite of several studies carried out in the second half of the last century, the issue of size-scale effects is not yet completely understood. The prescriptions provided by international design codes about the evaluation of the rotational capacity of RC elements (see e.g. Eurocode 2 [4] and the Model Code 90 [8]), in fact, do not take into account this effect.

In the case of concrete and rock specimens subjected to uniaxial compression, several experiments [32–37] reveal that the size-scale effects are due to two interconnected phenomena: the strain localization after the peak load and the subsequent energy dissipation over an internal surface, the value of which referred to a unitary surface can be considered as a material parameter. Based on these evidences, Carpinteri et al. [38, 39] have recently proposed to model the process of concrete crushing

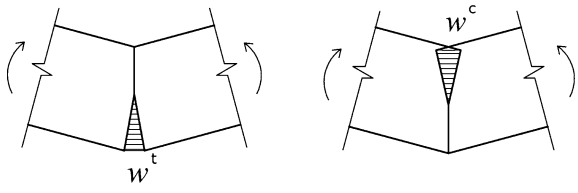

Fig. 2 Tensile fracture with cohesive zone (**a**); and analogous compression crushing with overlapping (**b**)

using an approach analogous to the *Cohesive Crack Model*, which is routinely adopted for modelling the tensile behaviour of concrete. This new approach is referred to as *Overlapping Crack Model* [38, 39] and assumes a stress-displacement law for the post-peak behaviour in compression (see Fig. 2).

On the other hand, the application of Fracture Mechanics concepts has been proved to be very effective for the analysis of size-scale effects in RC elements. Most of the applications concern the assessment of the shear resistance [40–43] and the evaluation of the minimum reinforcement [44–48].

In the present paper we propose a new numerical method able to describe the nonlinear behaviour of a RC members during both fracturing and crushing. Firstly, the *Cohesive Crack Model* for concrete in tension and the *Overlapping Crack Model* for concrete in compression are introduced, as well as a suitable stress-displacement relationship for steel in tension. Then, a numerical algorithm based on the finite element method is presented for the analysis of intermediate situations ranging from pure concrete members to over-reinforced beams. It is assumed that fracturing and crushing processes are fully localized along the mid-span cross-section of the representative concrete segment in bending. This assumption, fully consistent with the crushing phenomenon, also implies that only one equivalent main tensile crack is considered. Finally, a comparison between the numerical predictions and the results of several experimental tests carried out on RC beams in bending by Bosco and Debernardi [26], Bigaj and Walraven [27] and Pecce and Fabbrocino [10] is proposed in order to validate the new model.

2 Description of the proposed model

Let us consider a portion of a RC beam subjected to a bending moment M. This element, having a span to depth ratio equal to unity, is representative of the zone where a plastic hinge formation takes place. Note that the analysis of this structural element is consistent with the prescriptions reported in the Eurocode 2 [4] for the evaluation of the plastic rotation capacity of RC beams in bending. We also assume that the mid-span cross-section of this element is fully representative of its mechanical behaviour.

The stress distribution in the mid-span cross-section is linear-elastic until the tensile stress at the intrados reaches the concrete tensile strength. When this threshold is reached, a cohesive crack propagates from the beam intrados towards its extrados. Correspondingly, the applied moment increases. Outside the crack, the material is assumed to behave elastically. According to the well-known cohesive model, the stresses in the cohesive zone are assumed to be a function of the crack opening displacement and become equal to zero when the crack opening displacement is larger than a critical value. On the other hand, concrete crushing takes place when the maximum stress in compression reaches the concrete compression strength. After that, damage is described as an interpenetration of the two half-beams representing the localization of the dissipated energy (Fig. 3). Larger is the interpenetration, also referred to as overlapping in the sequel, lower are the transferred forces along the damaged zone.

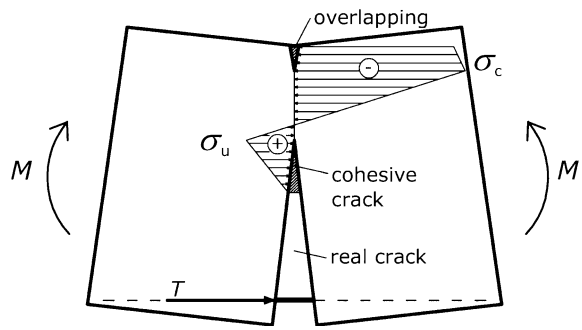

Fig. 3 Cohesive stress distribution in tension and fictitious overlapping in compression

2.1 Cohesive Crack Model for the description of concrete fracturing

A pioneering model for the analysis of nonlinear crack propagation in concrete was proposed by Hillerborg et al. [49] and Petersson [50] with the name of *Fictitious Crack Model*. Subsequently, an updated algorithm was implemented by Carpinteri [51, 52], with the terminology of *Cohesive Crack Model*, in order to study the ductile to brittle transition in plain concrete beams in bending. According to this model, the constitutive law used for the non-damaged zone is a $\sigma - \varepsilon$ linear-elastic relationship up to the achievement of the tensile strength, σ_u. In the process zone, the damaged material is still able to transfer a tensile stress across the crack surfaces. The cohesive stresses are considered to be decreasing functions of the crack opening, w^t, as follows:

$$\sigma = \sigma_u \left(1 - \frac{w^t}{w^t_{cr}}\right), \tag{1}$$

where w^t is the crack opening, w^t_{cr} is the critical value of the crack opening corresponding to $\sigma = 0$ and σ_u is the ultimate tensile strength of concrete. The area under the stress versus displacement curve represents the fracture energy, $\mathcal{G}_F$.

2.2 Overlapping Crack Model for the description of concrete crushing

The most frequently adopted constitutive laws for concrete in compression describe the material behaviour in terms of stress and strain (elastic-perfectly plastic, parabolic-perfectly plastic, Sargin's parabola, etc.). Such approaches imply that the energy is dissipated within a volume, whereas experimental results reveal that the energy is substantially dissipated over an internal surface as a result of strain localization [32–36]. Hillerborg [9] firstly proposed to model the crushing phenomenon as a strain localization over a specimen length proportional to the depth of the compressed zone. The Hillerborg's model is based on the definition of two different parameters: the critical value of the post-peak localized displacement in compression, w_c, that is a true material parameter, and the length over which the localization occurs. Such a length was not determined according to theoretical arguments and it was obtained through a best-fitting of experimental data. Moreover, this length is supposed to be proportional to the structural size. As a result, the obtained stress–strain curve is not a material property.

In the present formulation, we adopt the stress–displacement relationship proposed by Carpinteri et al. [38], and then considered also in Corrado [39], between the compression stress and the interpenetration, in close analogy with the cohesive model. The main hypotheses are:

(1) The constitutive law used for the undamaged material is a linear-elastic stress–strain relationship, see Fig. 4a.
(2) The crushing zone develops when the maximum compression stress reaches the concrete compression strength.
(3) The process zone is perpendicular to the main compression stress.
(4) The damaged material in the process zone is assumed to be able to transfer compression stresses between the overlapping surfaces. They are assumed to be decreasing functions of the interpenetration, w^c (see Fig. 4b):

$$\sigma = \sigma_c \left(1 - \frac{w^c}{w^c_{cr}}\right), \tag{2}$$

where w^c is the interpenetration, w^c_{cr} is the critical value of the interpenetration corresponding to $\sigma = 0$ and σ_c is the ultimate compression strength. This zone is then represented by a fictitious overlapping, which is mathematically analogous to the fictitious crack in tension, as shown in Fig. 2.

It is worth noting that, in the *Overlapping Crack Model*, only one parameter has to be defined: the critical value of overlapping, w^c_{cr}. This value can be directly obtained from experimental tests, see, e.g.,

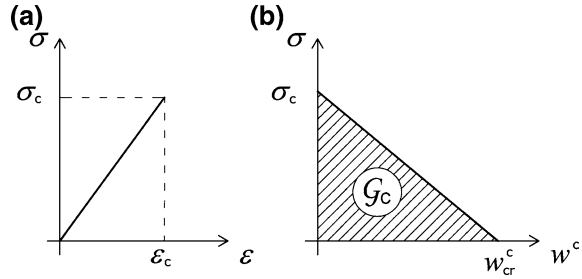

Fig. 4 Concrete constitutive laws in compression: $\sigma - \varepsilon$ linear-elastic law (**a**); $\sigma - w$ post-peak softening law (**b**)

the fundamental paper by Jansen and Shah [35]. The stress versus overlapping displacement curves of specimens characterized by different slenderness or size, in fact, tend to collapse onto a single curve, whereas they are totally different in a classical stress–strain diagram. From such data, the critical value of overlapping, w_{cr}^{c}, can be univocally defined as the interpenetration corresponding to $\sigma = 0$. Similarly, the crushing energy, $\mathcal{G}_C$, is defined as the area below the post-peak softening curve (see Fig. 4b), and it is a true material parameter, since it is not affected by the structural dimension. Dahl and Brincker [33] carried out a series of uniaxial compression tests with the aim of measuring the dissipated energy per unit cross sectional area. They obtained values of about 50 N/mm and claimed that this dissipated energy becomes independent of the specimen size if the specimen is large enough. An empirical formulation for calculating the crushing energy has recently been proposed by Suzuki et al. [53], based on the results of compression tests carried out on plain and transversal reinforced concrete specimens. In the present study, the crushing energy is computed according to the following empirical equation, which considers the confined concrete compression strength by means of the stirrups yield strength and the stirrups volumetric content:

$$\frac{\mathcal{G}_C}{\sigma_c} = \frac{\mathcal{G}_{C,0}}{\sigma_c} + 10,000\frac{k_a^2 p_e}{\sigma_c^2}, \tag{3a}$$

where σ_c is the average concrete compression strength, k_a is a parameter depending on the stirrups strength and volumetric percentage and p_e is a coefficient related to the effective lateral pressure (see Suzuki et al. [53]). The crushing energy for unconfined concrete, $\mathcal{G}_{C,0}$, can be calculated using the following expression:

$$\mathcal{G}_{C,0} = 80 - 50k_b, \tag{3b}$$

where the parameter k_b depends on the concrete compression strength [53].

By varying the concrete compression strength from 20 to 90 MPa, Eq. 3b gives a crushing energy ranging from 30 to 58 N/mm. It is worth noting that $\mathcal{G}_C$ is between two and three orders of magnitude higher than $\mathcal{G}_F$, and that the critical values for crushing interpenetration and crack opening are approximately equal to $w_{cr}^{c} \approx 1$ mm (see also the experimental results in [35]) and $w_{cr}^{t} \approx 0.1$ mm, respectively. Finally, we remark that, in the case of concrete confinement, the crushing energy, computed using Eq. 3a, and the corresponding critical value for crushing interpenetration, considerably increase.

2.3 Steel-concrete interaction

In order to model the steel contribution to the load carrying capacity of the beam, it is necessary to introduce a suitable bond-slip law for the characterization of steel-concrete interaction. Typical bond-slip relationships are defined in terms of a tangential stress along the steel-concrete interface as a function of the relative tangential displacement between the two materials [8, 54–57]. The integration of the differential slip over the transfer length, l_{tr}, is equal to one half of the opening crack at the reinforcement level. On the other hand, the integration of the bond stresses gives the reinforcement reaction. In order to simplify the calculation, the stress-displacement law is herein assumed to be linear until the yield stress—or until the critical crack opening for steel, w_y—is achieved. After that, the reinforcement reaction is considered to be constant, until the crack opening displacement at the reinforcement level reaches a limit value corresponding to steel failure.

3 Numerical algorithm

A discrete form of the elastic equations governing the mechanical response of the two half-beams is herein introduced in order to develop a suitable algorithm for the analysis of intermediate situations where both fracturing and crushing phenomena take place. The mid-span cross-section of the beam can be subdivided into finite elements by n nodes (Fig. 5). In this scheme, cohesive and overlapping stresses are replaced by equivalent nodal forces, F_i, by integrating the corresponding tractions over each element size. Such nodal forces depend on the nodal opening or closing displacements according to the cohesive or overlapping softening laws previously introduced.

The horizontal forces, F, acting along the mid-span cross-section can be computed as follows:

$$\{F\} = [K_w]\{w\} + \{K_M\}M \tag{4}$$

where $\{F\}$ is the vector of nodal forces, $[K_w]$ is the matrix of the coefficients of influence for the nodal

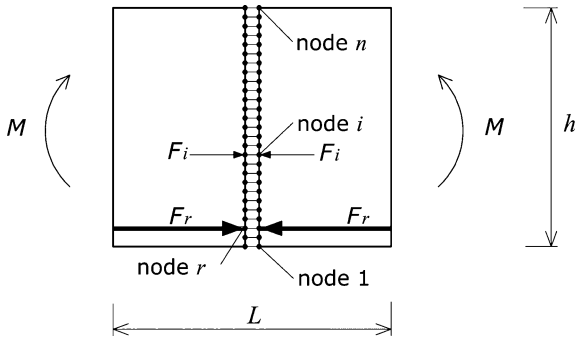

Fig. 5 Finite element nodes along the middle cross-section

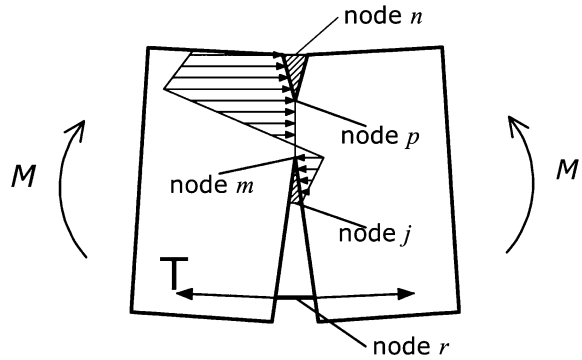

Fig. 6 Force distribution with cohesive crack in tension and fictitious crushing in compression

displacements, $\{w\}$ is the vector of nodal displacements, $\{K_M\}$ is the vector of the coefficients of influence for the applied moment, and M is the applied moment. Equation 4 permits to analyse the fracturing and crushing processes of the mid-span cross-section taking into account the elastic behaviour of the RC member. To this aim, all the coefficients are computed a priori using a finite element analysis. Due to the symmetry of the problem, a homogeneous concrete rectangular region, corresponding to half the tested specimen, is discretized by means of quadrilateral plane stress elements with uniform nodal spacing. Horizontal constraints are then applied to the nodes along the vertical symmetry edge. Each coefficient $K_w^{i,j}$ entering Eq. 4, which relates the nodal force F_j to the nodal displacement w_i, have the physical dimensions of a stiffness and are computed by imposing a unitary horizontal displacement to each of the constrained nodes. On the other hand, by applying a unitary external bending moment, it is possible to compute the coefficients K_M^i. They have the physical dimensions of $[L]^{-1}$.

The reinforcement contribution is also included in the nodal force corresponding to the r-th node.

In the generic situation shown in Fig. 6, the following equations can be considered:

$$F_i = 0; \quad \text{for i} = 1, 2, \ldots, (j-1);\ i \neq r \tag{5a}$$

$$F_i = F_u\left(1 - \frac{w_i^t}{w_{cr}^t}\right); \quad \text{for i} = j, \ldots, (m-1);\ i \neq r \tag{5b}$$

$$w_i = 0; \quad \text{for i} = m, \ldots, p \tag{5c}$$

$$F_i = F_c\left(1 - \frac{w_i^c}{w_{cr}^c}\right); \quad \text{for i} = (p+1), \ldots, n \tag{5d}$$

$$F_i = f(w_i); \quad \text{for i} = r. \tag{5e}$$

where j represents the real crack tip, m represents the fictitious crack tip, p is the fictitious overlapping tip and r is the node corresponding to the steel reinforcement.

Equation 5e represents the relationship between the closing force exerted by the reinforcing steel and the crack opening at the reinforcement level. Such a law is determined on the basis of the bond-slip behaviour of concrete and steel. It is worth noting that, in this framework, it is possible to insert a reinforcement in compression by introducing a suitable stress-displacement constitutive law in the corresponding node. Due to lack of studies on the behaviour of reinforcing bars in compression, the $\sigma - w$ relationship adopted is the same as that used for steel in tension.

Equations 4 and 5 constitute a linear algebraic system of $(2n)$ equations in $(2n + 1)$ unknowns, namely $\{F\}$, $\{w\}$ and M. A possible additional equation can be chosen: we can set either the force in the fictitious crack tip, m, equal to the ultimate tensile force, or the force in the fictitious crushing tip, p, equal to the ultimate compression force. In the numerical scheme, we choose the situation which is closer to one of these two possible critical conditions. This criterion will ensure the uniqueness of the solution on the basis of physical arguments. The driving parameter of the process is the tip that in the considered step has reached the limit resistance. Only this tip is moved when passing to the next step.

The two fictitious tips advance until they converge to the same node. So forth, in order to describe the descending branch of the moment-rotation diagram, the two tips can move together towards the intrados of the beam. As a consequence, the crack in tension closes and the overlapping zone is allowed to extend towards the intrados. This situation is quite commonly observed in over-reinforced beams, where steel yielding does not take place.

Finally, at each step of the algorithm, it is possible to calculate the beam rotation, ϑ, as follows:

$$\vartheta = \{D_w\}^{\mathrm{T}}\{w\} + D_M M \tag{6}$$

where D_w^{i} is the coefficient of influence for the nodal displacements, obtained through the finite element analysis as the rotation of the free edge corresponding to a unitary displacement of the i-th constrained node and it has the physical dimensions of $[\mathrm{L}]^{-1}$. D_M is the coefficient of influence for the applied moment with physical dimensions of $[\mathrm{F}]^{-1}$ $[\mathrm{L}]^{-1}$.

As regards the analysis of size-scale effects, the coefficients entering Eqs. 4 and 6 are connected by a simple relation of proportionality to the structural dimension. This means that it is not necessary to repeat the finite element analysis for any different considered beam size. More precisely, if all the three specimen sizes (depth h, span L, thickness b) are multiplied by the factor k, the coefficients are transformed as follows:

$$K_w^{\mathrm{i,j}}(kd) = kK_w^{\mathrm{i,j}}(d), \tag{7a}$$

$$K_M^{\mathrm{i}}(kd) = \frac{1}{k}K_M^{\mathrm{i}}(d), \tag{7b}$$

$$D_w^{\mathrm{i}}(kd) = \frac{1}{k}D_w^{\mathrm{i}}(d), \tag{7c}$$

$$D_M(kd) = \frac{1}{k^3}D_M(d). \tag{7d}$$

4 Comparison between model predictions and experimental results

In this section, the comparison between the numerical predictions and the experimental results of three different testing programmes is carried out. In the numerical scheme, the mid-span cross-section of the central portion of the RC beams is discretized into 160 finite elements and the coefficients of influence entering Eq. 4 are preliminary determined using the finite element method.

4.1 Tests by Bosco and Debernardi

The first testing programme herein considered was carried out by Bosco and Debernardi in the Materials and Structures Laboratory of the Department of Structural Engineering and Geotechnics of the Politecnico di Torino on 22 simply supported RC beams [26]. Three different structural scales of the beams were considered, with cross-section depths of 200, 400 and 600 mm and constant slenderness $L/h = 10$. The percentage of tensile reinforcement, ρ_{t}, was varied between 0.13 and 1.70%. The characteristics of stirrups and compression reinforcement, ρ_{c}, are given in Table 1. The width to depth ratio of the beam cross-section, $b/h = 0.5$, the effective depth to total depth ratio, $d/h = 0.9$ and the diameter of the tension bars, $\phi = 12$ mm, were kept constant. The instrumentation included two linear potentiometers (devices 7 and 12 in Fig. 7) for measuring the deformations at the top and bottom sides of the beam. The length of each extensimeter was equal to the beam depth. By means of such an instrumentation, the rotation of the mid-span region, characterized by a length equal to the depth, can be directly evaluated as the difference between the longitudinal displacements at the intrados and at the extrados, divided by the total beam depth. The reinforcing bars have the following mechanical parameters: yield strength,

Table 1 Mechanical and geometrical parameters of the beams tested by Bosco and Debernardi [26]

Beam	h (mm)	b (mm)	L (mm)	ρ_{t} (%)	ρ_{c} (%)	Stirrups	$\mathcal{G}_{\mathrm{C}}$ (N/mm)
T1	200	100	2,000	0.57	0.25	ϕ 6/150	53
T2				1.13	0.50	ϕ 6/150	
T3				1.71	0.50	ϕ 6/150	
T4	400	200	4,000	0.28	0.20	ϕ 6/200	30
T5				0.57	0.20	ϕ 6/200	
T6				1.13	0.20	ϕ 6/200	
T7				1.71	0.20	ϕ 6/200	
T8	600	300	6,000	0.13	0.12	ϕ 6/150	48
T9				0.25	0.12	ϕ 6/150	
T10				0.57	0.12	ϕ 6/150	
T11				1.13	0.12	ϕ 6/150	

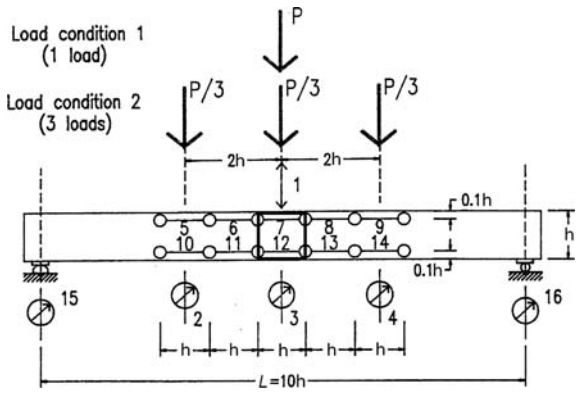

Fig. 7 Testing scheme and loading conditions in Bosco and Debernardi [26]

$f_{ym} = 587$ N/mm^2, failure stress, $f_{tm} = 672$ N/mm^2 and strain at failure load, $\varepsilon_{su} = 7.0\%$. The mean compression strength of concrete, was equal to 30.9 N/mm^2. The average concrete tensile strength, evaluated by splitting tensile tests was equal to 2.97 N/mm^2. The outcome of the testing programme is represented by the bending moment versus rotation diagram of the central portion of the beams.

The numerical simulations have been carried out by modelling the central beam region characterized by a span to depth ratio equal to unity, in order to obtain a consistent comparison with experimental measures (see Fig. 7). The values of the crushing energy, determined according to Eq. 3a taking into account the stirrups confinement, are reported in Table 1. The numerical and experimental moment-rotation curves are compared in Fig. 8 for different beam depths and different steel percentages. These diagrams put into evidence that the maximum rotation is a decreasing function of the tensile reinforcement ratio and of the beam depth. In the case of low steel percentages, the mechanical behaviour is characterized by reinforcement yielding and the mechanical response is almost plastic. By increasing the amount of reinforcement, the contribution of concrete crushing becomes more and more evident with the appearance of a softening branch at the end of the plastic plateau. This is an important feature of the proposed model, which also permits to follow unstable softening branches with positive slopes (snap-back). This is made possible by controlling the loading process through the length of the tensile crack and the extension of the fictitious crushing zone, rather than by the external load or the global rotation. The numerically predicted maximum resistant moments are very often lower than the experimental ones, as we can see in Fig 8a–c. This is due to the fact that in the numerical model the hardening behaviour of steel before yielding is not taken into account. On the other hand, a good agreement is obtained with the ultimate resistant moment calculated in accordance with the Eurocode 2 prescriptions (parabolic-perfectly plastic relationship for concrete in compression and elasto-plastic relationship for steel), whose values are reported with dashed lines in Fig. 8a–c. The size-scale effect is put into evidence in Fig. 8d by keeping constant the steel percentage equal to 1.13% and varying the beam depth from 200 to 600 mm. A general good agreement is obtained between numerical and experimental results for all the tested beams.

4.2 Tests by Bigaj and Walraven

The second testing programme herein considered is that carried out by Bigaj and Walraven in the Stevin Laboratory of the Delft University of Technology [27]. The main parameters investigated were the member size and the reinforcement ratio. In particular, three different dimensional classes of beams with effective depths of 90, 180 and 450 mm and slenderness equal to 11 were tested in three-point-bending configuration. Two different steel percentages were analysed, having $\rho_t = 0.28\%$ and $\rho_t = 1.12\%$, as shown in Fig. 9. The main geometrical and mechanical parameters of the tested beams are given in Table 2. The mechanical parameters of reinforcement were different for each bar diameter. The mean concrete compression strength, determined on 28 days standard cubes, was equal to 35 N/mm^2. The instrumentation permitted to measure the displacement at the mid-span and the total rotation of the beam, calculated by integration of the curvature along the longitudinal axis of the member for each loading step. Both the reinforcement in compression and the stirrups were absent.

In this case, the experimental results are represented by the applied load as a function of the total plastic rotation evaluated on the whole beam. Since the numerical simulation is referred to a beam region with a span to depth ratio equal to unity, we assume that the development of ductility is localized within such a region. The comparison between numerical

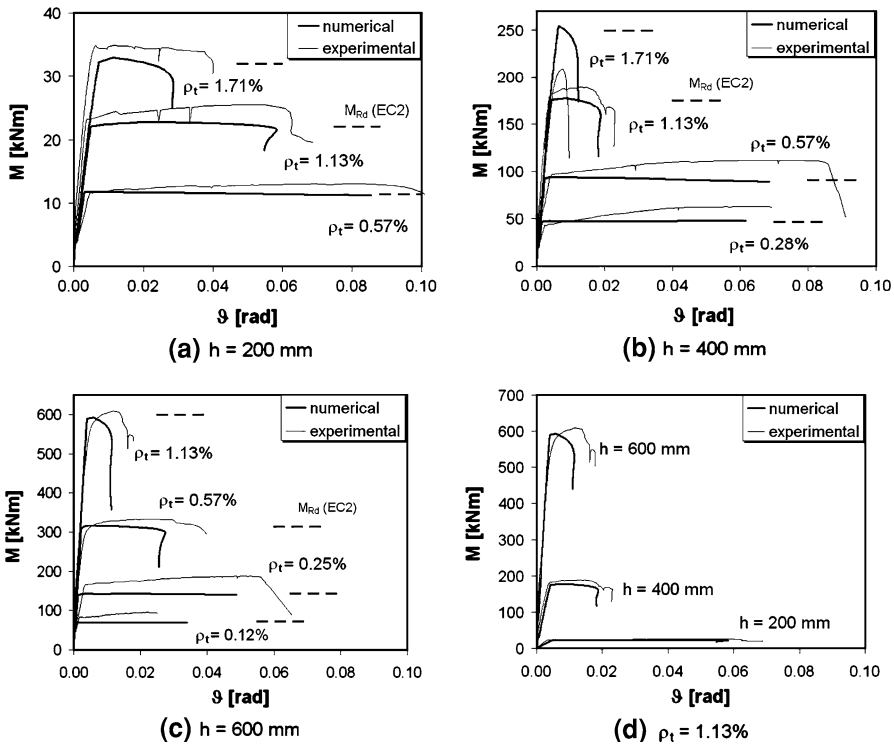

Fig. 8 Numerical and experimental moment versus rotation diagrams for the beams tested by Bosco and Debernardi [26]

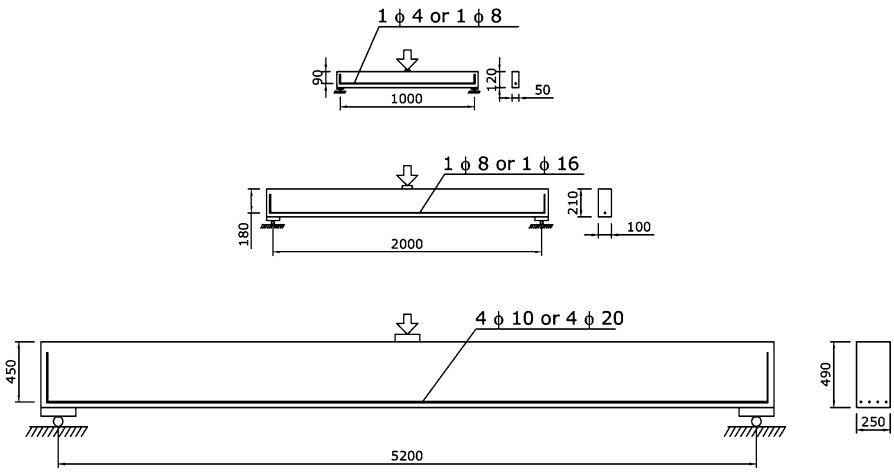

Fig. 9 Dimensional classes of beams tested by Bigaj and Walraven [27]

and experimental plastic rotations as a function of the beam depth is shown in Fig. 10. In the case of steel percentage equal to 0.28%, a good agreement is obtained, whereas a larger difference appears for the amount of reinforcement equal to 1.12%, although the trend is correctly reproduced. This discrepancy is due to the fact that in the numerical approach the plastic rotation is defined as $\vartheta_{PL}^{(2)}$ in Fig. 1, whereas in the experimental programme the plastic rotation was computed as $\vartheta_{PL}^{(1)}$ in Fig. 1. A more detailed analysis would require a numerical-experimental comparison between the load-deflection diagrams. However this is not possible to do for all the tested beams, because only the data of two cases are available (see Fig. 11).

The total numerical mid-span deflection is computed as the sum of the elastic contribution, calculated with a reduced elastic modulus in order to take into account the stiffness reduction due to smeared cracking, and the contribution given by the localized rotation of the mid-span portion, as in [58].

Table 2 Mechanical and geometrical parameters of the beams tested by Bigaj and Walraven [27]

Beam	h (mm)	d (mm)	b (mm)	L (mm)	ρ_t	(%)
B.0.1	120	90	50	1,000	1ϕ4	0.28
B.0.2	210	180	100	2,000	1ϕ8	
B.0.3	490	450	250	5,000	4ϕ10	
B.1.1	120	90	50	1,000	1ϕ8	1.12
B.1.2	210	180	100	2,000	1ϕ16	
B.1.3	490	450	250	5,000	4ϕ20	

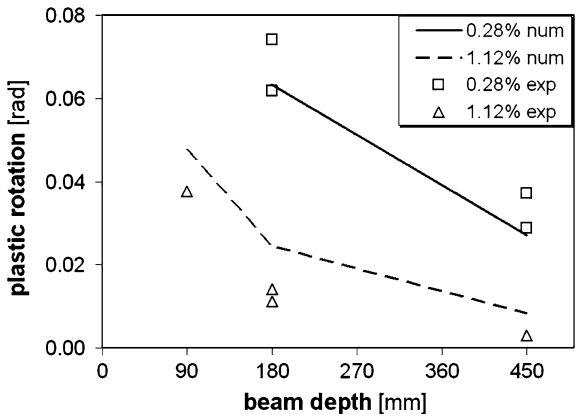

Fig. 10 Numerical and experimental plastic rotation versus beam depth for the beams tested by Bigaj and Walraven [27]

A good agreement is obtained between the numerical and the experimental load-deflection curves for both $\rho_t = 0.28\%$ and $\rho_t = 1.12\%$ (see Fig. 11). It is worth noting that the two points corresponding to the definitions of plastic rotation, $\delta_{u,NUM}$ and $\delta_{u,EXP}$, are very close to each other in the case of low steel percentage, whereas they are very different in the case of high reinforcement percentage.

Table 3 Mechanical and geometrical parameters of the beams tested by Pecce and Fabbrocino [10]

Beam	h (mm)	b (mm)	L (mm)	σ_c (MPa)	ρ_t (%)	ρ_c	Stirrups
A	180	400	3,200	41.8	2.6	2 ϕ 6	ϕ 8/100
AH				94.6			
B	180	400	3,200	41.8	1.1		
BH				94.6			
C	520	320	5,000	41.8	2.2		
CH				94.6			

4.3 Tests by Pecce and Fabbrocino

Finally, the experimental programme carried out by Pecce and Fabbrocino at the University of Naples, on 20 simply supported RC beams [10] is considered. Three different combinations of beam dimensions and reinforcement arrangement were used, as reported in Table 3. Two different types of concrete were considered: a normal strength concrete, with a compression strength, σ_c, equal to 41.8 N/mm^2, and a high strength concrete, with a compression strength equal to 94.6 N/mm^2. The steel was characterized by a yield stress, f_y, equal to 480 N/mm^2 and a deformation at failure, ε_u, equal to 13%. The percentage of steel in compression and the amount of stirrups are reported in Table 3. The outcome of the testing programme is represented by the applied load versus total rotation for each tested beam. In this case the total rotation is evaluated as the sum of the rotations at the supports, as schematically shown in Fig. 12. The choice of variables of such experimental programme allows to investigate on the influence of the geometrical and mechanical percentage of reinforcement, on the concrete grade and on the beam slenderness, L/h.

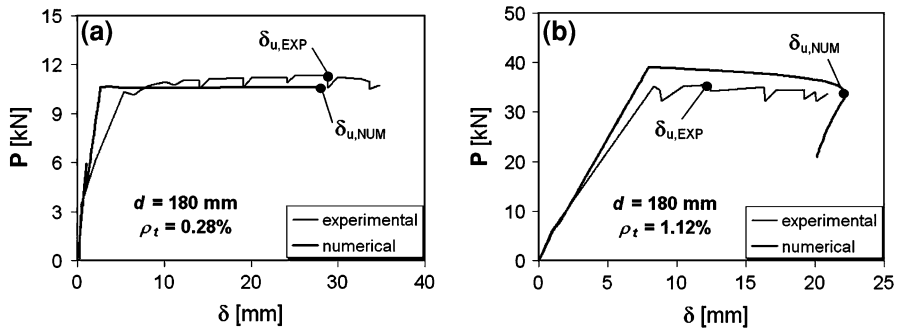

Fig. 11 Numerical and experimental applied load versus mid-span deflection diagrams for two of the beams tested by Bigaj and Walraven [27]

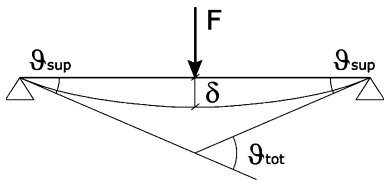

Fig. 12 Evaluation of the total rotation in Pecce and Fabbrocino [10]

The numerical predictions and the experimental results are compared in Fig. 13 in terms of the applied load versus total beam rotation. Since the numerical analysis is carried out on the mid-span region of the beam with a depth to length ratio equal to the unity, the good agreement obtained for $\rho_t = 2.6\%$ and $\rho_t = 2.2\%$ (see Fig. 13a, b, e, f) confirms that the ductility of over-reinforced concrete beams is mainly localized in the mid-span position of the beam, where concrete crushing takes place. On the contrary, in the case of lower reinforcement percentages, as, e.g., for $\rho_t = 1.1\%$, the crack pattern is more diffuse and the total rotation is higher than the rotation of the mid-span portion (see Fig. 13c, d).

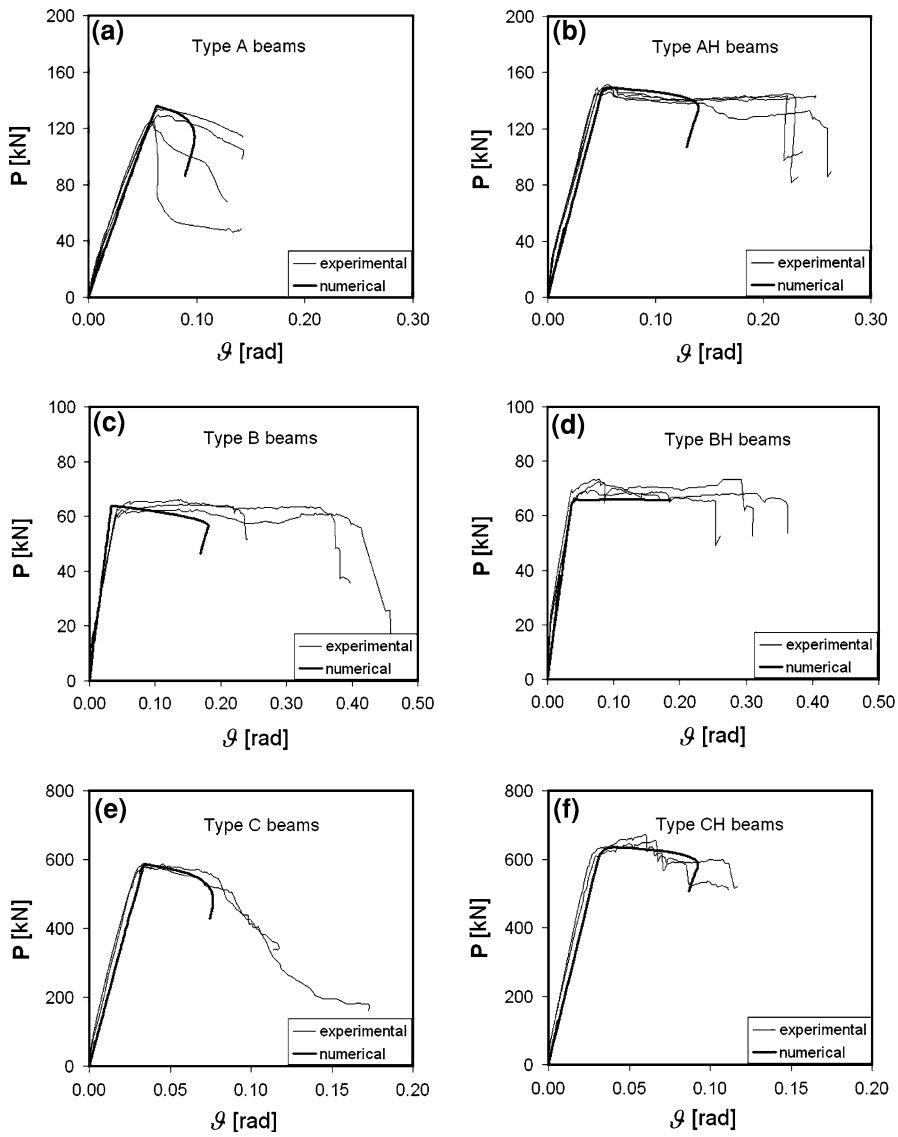

Fig. 13 Numerical and experimental applied load versus total rotation diagrams for the beams tested by Pecce and Fabbrocino [10]

5 Discussion and conclusions

In the present paper, a numerical algorithm has been proposed for the analysis of the behaviour of RC elements in bending. To this aim, all the main nonlinear contributions have been taken into account for an accurate evaluation of the moment-rotation diagram: concrete fracturing in tension, which produces effects in the rising part of the moment-rotation diagram; steel yielding or slippage, which determines a rapid increment in the beam rotation with a resistant moment almost constant; and concrete crushing in compression, which is the reason for the observed descending branch at the end of the horizontal plateau (see the qualitative diagram in Fig. 1). This latter nonlinearity, which highly depends on the size-scale of the specimen, is fundamental for the prediction of the ultimate rotation, since it delimits the plastic plateau (see the comparison with experimental results in Figs. 8 and 13). Therefore, among the various forms of nonlinearity, concrete crushing plays a key role for the evaluation of the rotational capacity. In over-reinforced beams, in fact, the development of crushing failure is responsible for a very sudden loss in the load-carrying capacity, with the appearance of a severe snap-back instability. With this tool in hand, the simulation of the mechanical behaviour of all the intermediate situations, ranging from pure concrete to over-reinforced concrete beams, can be obtained. The following main conclusions can be drawn from the comparison between numerical predictions and experimental results.

(1) The introduced constitutive law for concrete in compression through the *Overlapping Crack Model* allows for the description of the nonlinear behaviour of concrete considering the effect of the structural dimension. In particular, as shown in Figs. 8 and 10, it is possible to state that, independent of the reinforcement ratio, the rotational capacity of RC beams in bending is a decreasing function of the beam depth. This is very well evidenced by a progressive reduction of the beam rotation at failure.

(2) By varying the steel percentage, a double transition is evidenced: a brittle behaviour in the case of very low steel percentages due to tensile crack propagation, a ductile behaviour in the case of medium steel percentages, and again a brittle response for high steel percentages, due to concrete crushing.

(3) The numerical model, controlling the loading process through the length of the tensile crack and the extension of the fictitious crushing zone, permits to describe the descending branch of the moment-rotation diagram experimentally evidenced in the case of over-reinforced beams, as shown in Figs. 8 and 13.

(4) In the case of high steel percentage, as, e.g., for $\rho_t = 2.6\%$, the contribution on the global ductility is localised in the mid-span region, where concrete crushing takes place.

(5) In order to fully describe the experimental results, it is essential to consider the contribution of the reinforcement in compression and the stirrups confinement on the mechanical behaviour of RC beams, as well as the actual value of the concrete compression strength. In general, we can assert that the ductility—expressed by means of the maximum rotation—is an increasing function of the reinforcement ratio in compression, since the latter determines a reduction of concrete crushing. An analogous effect is due to the concrete compression strength, as it can be deduced from the diagrams shown in Fig. 13. Also the transversal reinforcement influences the ductility, through an improvement of concrete confinement, with a consequent increment of the ultimate strain. In the proposed model, this effect was taken into account by increasing the critical value of the overlapping displacement and of the crushing energy.

Finally, a comparison between the calculated plastic rotations and the experimental values of the all testing programmes considered in this paper is shown in Fig. 14a. Since the experimental results usually exhibit a large scatter (see also Siviero [3]), a rather satisfactory result is obtained. Besides, this result is in agreement with that obtained by the analytical model of Eligehausen et al. [59] and shown in Fig. 14b. On the other hand, it has to be emphasized that the model by Eligehausen permits to evaluate in depth the influence of steel-concrete interaction, steel ductility class and reinforcement arrangement on the rotational capacity of RC beams in bending, whereas it is not effective for the assessment of size effects, since it is

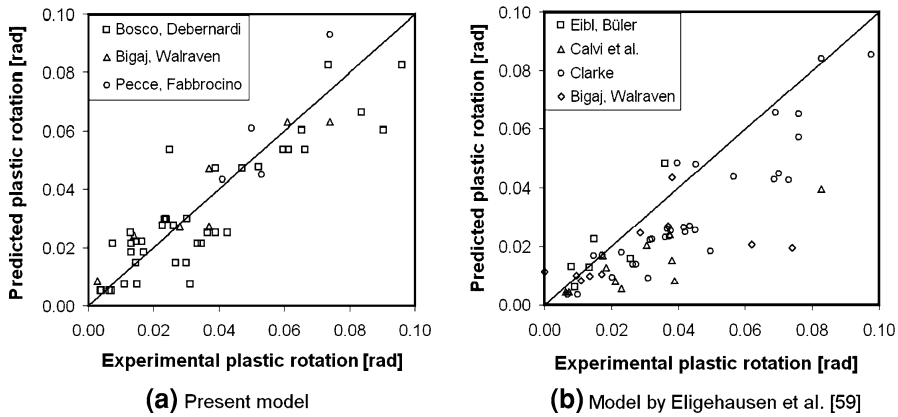

Fig. 14 Comparison between predicted and experimental plastic rotations

based on stress–strain relationships for concrete in tension and compression. On the contrary, the model by Hillerborg [9] addresses the problem of size effects, but it is based on the localization length, which is determined by means of a best fitting procedure on experimental data. For this reason, it is not a useful tool for prediction. Besides, the original model by Hillerborg cannot be used to simulate the experimental tests considered in this paper, since it does not consider the reinforcement in compression, as well as the effect of stirrups confinement. For such reasons, a comparison with the Hillerborg's model has not been performed.

Acknowledgements The financial support provided by the European Union to the Leonardo da Vinci Project 2006-I/06/B/F/PP-154069 "Innovative Learning and Training on Fracture" (ILTOF) is gratefully acknowledged.

References

1. Baker ALL (1956) The ultimate load theory applied to the design of reinforced and prestressed concrete frames. Concrete Publications Ltd., London
2. Macchi G (1969) Limit-states design of statically indeterminate structures composed of linear members. Costruzioni in Cemento Armato. Studi e Rendiconti 6: 151–191
3. Siviero E (1974) Rotation capacity of monodimensional members in structural concrete. CEB Bulletin d'Information 105:206–222
4. EN 1992-1-1 (2003) Eurocode 2: design of concrete structures—Part 1–1: general rules and rules for buildings
5. prEN 1998-1 (2003) Eurocode 8: design of structures for earthquake resistance—Part 1: general rules, seismic action and rules for buildings
6. Macchi G (1956) Sulla ridistribuzione plastica dei momenti nelle travi iperstatiche. Accademia Nazionale dei Lincei VIII(12)
7. Baker ALL (1966) Simplified bi-linear limit design. Structures hyperstatiques, Projet d'annexe aux Recommandations Pratiques, CEB 1966
8. Comité Euro-International du Béton (1993) CEB-FIP Model Code 1990. Bulletin d'Information 213/214
9. Hillerborg A (1990) Fracture mechanics concepts applied to moment capacity and rotational capacity of reinforced concrete beams. Eng Fract Mech 35:233–240. doi: 10.1016/0013-7944(90)90201-Q
10. Pecce M, Fabbrocino G (1999) Plastic rotation capacity of beams in normal and high-performance concrete. ACI Struct J 96:290–296
11. Eligehausen R, Langer P (1987) Rotation capacity of plastic hinges and allowable moment redistribution. CEB Bulletin d'Information 175:I 7.9–I 7.27
12. Clarke JL (1990) The ductility of reinforcement and its influence on the rotation capacity of concrete sections. Project report no. RE1.019.00.2, Project for Fabric Reinforcement Development Association, British Cement Association
13. Calvi GM, Cantù E, Macchi G, Magenes G (1993) Rotation capacity of r.c. slabs as a function of steel properties. CEB Bulletin d'Information 218:45–64
14. Beeby AW (1997) Ductility in reinforced concrete: why is it needed and how is it achieved? Struct Eng 75:311–318
15. Dilger W (1966) Veränderlichkeit der Biege- und Schubtragfähigkeit bei Stahlbetontragwerken und ihr Einfluß auf Schnittkraftverteilung und Traglast bei statisch unbestimmter Lagerung. DAfStb Heft 179, Berlin
16. Bachmann H (1970) Influence of shear and bond on rotation capacity of reinforced concrete beams. IABSE Publications 30-II
17. Langer P (1987) Verdrehfähigkeit Plastizierter Tragwerksbereiche im Stahlbetonbau. PhD Thesis, University of Stuttgart, Institut für Werkstoffe im Bauwesen, published in DAfStb, Berlin
18. Sveinson T, Dilger WH (1991) Moment redistribution in reinforced concrete structures. University of Waterloo Publication, Waterloo

19. Sigrist V, Marti P (1994) Ductility of structural concrete: a contribution. Workshop on development of EN 1992 in relation to new research results and the CEB-FIP Model Code 1990, Czech Technical University, Prague, pp 211–223
20. Shin S, Ghosh SK, Moreno J (1989) Flexural ductility of ultra-high-strength concrete members. ACI Struct J 86: 394–400
21. Markeset G (1993) Failure of concrete under compressive strain gradients. PhD Thesis, The Norwegian Institute of Technology, Trondheim
22. Burns NH, Siess CP (1966) Plastic hinging in reinforced concrete. J Struct Div 92:45–61
23. Somes NF (1966) Technical report: moment-rotation characteristics of prestressed concrete members, Stage I: rectangular sections. TRA/398, Cement and Concrete Association, London, England
24. Mattock AH (1965) Rotational capacity of hinging regions in reinforced concrete beams. In: Abstracts of the flexural mechanics of reinforced concrete, ASCE-ACI International Symposium, ACI SP-12, pp 143–181
25. Corley GW (1966) Rotational capacity of reinforced concrete beams. J Struct Div 92:121–146
26. Bosco C, Debernardi PG (1992) Experimental investigation on the ultimate rotational capacity of R.C. beams. Report no. 36, Atti del Dipartimento, Politecnico di Torino, Ingegneria Strutturale
27. Bigaj A, Walraven JC (1993) Size effect on rotational capacity of plastic hinges in reinforced concrete beams. CEB Bulletin d'Information 218:7–23
28. Cosenza E, Greco C, Manfredi G (1991) La valutazione teorica di spostamenti e rotazioni in fase anelastica negli elementi monodimensionali in cemento armato. Atti dell'Accademia Nazionale dei Lincei IX(2):249–258 (in Italian)
29. Tue N, Qian L, Pommerening D (1996) Abschlußbericht zum Forschungs vorhaben Duktilitätsanforderungen en vorgespannte Tragwerke im Hoch-, Grund- und Brückenbau. Technische Hochschule Darmstadt, Az. IV 1-5-683/92
30. Bigaj AJ, Walraven J (2002) Size effects on plastic hinges of reinforced concrete members. Heron 47:53–75
31. Fantilli AP, Iori I, Vallini P (2007) Size effect of compressed concrete in four point bending RC beams. Eng Fract Mech 74:97–108. doi:10.1016/j.engfracmech.2006.01.013
32. Van Mier JGM (1984) Strain softening of concrete under multiaxial compression, PhD Thesis, Eindhoven University of Technology, The Netherlands
33. Dahl H, Brincker R (1989) Fracture energy of high-strength concrete in compression. In: Shah SP, Swartz SE, Barr B (eds) Fracture of concrete and rock—recent developments. Proceedings of the international conference on recent developments in the fracture of concrete and rock, Cardiff, Wales, 1989. Elsevier Applied Science, England, pp 523–536
34. Van Vliet M, Van Mier J (1996) Experimental investigation of concrete fracture under uniaxial compression. Mech Cohesive Frict Mater 1:115–127. doi:10.1002/(SICI)1099-1484(199601)1:1<115::AID-CFM6>3.0.CO;2-U
35. Jansen DC, Shah SP (1997) Effect of length on compressive strain softening of concrete. J Eng Mech 123:25–35. doi:10.1061/(ASCE)0733-9399(1997)123:1(25)
36. Ferrara G, Gobbi ME (1995) Strain softening of concrete under compression. Report to RILEM Committee 148-SSC, ENEL-CRIS Laboratory, Milano, Italy
37. Hudson JA, Brown ET, Fairhurst C (1972) Shape of the complete stress–strain curve for rock. In: Cording EJ (ed) Proceedings of the 13th symposium on rock mechanics, University of Illinois, Urbana, Illinois, 1971, American Society of Civil Engineers, pp 773–795
38. Carpinteri A, Corrado M, Paggi M, Mancini G (2007) Cohesive versus overlapping crack model for a size effect analysis of RC elements in bending. In: Carpinteri A, Gambarova P, Ferro G, Plizzari G (eds) Fracture mechanics of concrete structures. Proceedings of the 6th international FraMCoS conference, Catania, Italy, 2007, vol 2. Taylor & Francis, London, pp 655–663
39. Corrado M (2007) Effetti di scala sulla capacità di rotazione plastica di travi in calcestruzzo armato, PhD Thesis, Politecnico di Torino (in Italian)
40. Gustafsson PJ, Hillerborg A (1988) Sensitivity in shear strength of longitudinally reinforced concrete beams energy of concrete. ACI Struct J 85:286–294
41. Jenq YS, Shah SP (1989) Shear resistance of reinforced concrete beams—a fracture mechanics approach. In: Li VC, Bazant ZP (eds) Fracture mechanics: application to concrete (special report ACI SP-118), American Concrete Institute, Detroit, pp 327–358
42. Bazant ZP, Kim JK (1984) Size effect in shear failure of longitudinally reinforced beams. ACI J 81:456–468
43. Carpinteri A, Ventura G, Carmona JR (2007) Flexural to shear and crushing failure transitions in RC beams by the bridged crack model. In: Carpinteri A, Gambarova P, Ferro G, Plizzari G (eds) Fracture mechanics of concrete structures. Proceedings of the 6th International FraMCoS Conference, Catania, Italy, 2007, vol 2. Taylor & Francis, London, pp 677–684
44. Carpinteri A (1981) A fracture mechanics model for reinforced concrete collapse. In: Advanced mechanics of reinforced concrete. Proceedings of a IABSE colloquium, Delft, the Netherlands, 1981. Delft University Press, Delft, pp 17–30
45. Carpinteri A (1984) Stability of fracturing process in RC beams. J Struct Eng 110:544–558
46. Bosco C, Carpinteri A, Debernardi PG (1990) Minimum reinforcement in high-strength concrete. J Struct Eng 116:427–437. doi:10.1061/(ASCE)0733-9445(1990)116:2(427)
47. Carpinteri A (ed) (1999) Minimum reinforcement in concrete members. Elsevier Science Ltd., Oxford, UK
48. Appa Rao G, Vijayanand I, Eligehausen R (2008) Studies on ductility and evaluation of minimum flexural reinforcement in RC beams. Mater Struct 41(4):759–771. doi:10.1617/s11527-007-9280-7
49. Hillerborg A, Modeer M, Petersson PE (1976) Analysis of crack formation and crack growth in concrete by means of fracture mechanics and finite elements. Cement Concr Res 6:773–782. doi:10.1016/0008-8846(76)90007-7
50. Petersson P (1981) Crack growth and development of fracture zones in plain concrete and similar materials. Report TVBM-1006, Division of Building Materials, Lund Institute of Technology

51. Carpinteri A (1985) Interpretation of the Griffith instability as a bifurcation of the global equilibrium. In: Shah SP (ed) Application of fracture mechanics to cementitious composites. NATO advanced research workshop, Evanston, USA, 1984. Martinus Nijhoff Publishers, Dordrecht, pp 287–316
52. Carpinteri A (1989) Size effects on strength, toughness, and ductility. J Eng Mech 115:1375–1392
53. Suzuki M, Akiyama M, Matsuzaki H, Dang TH (2006) Concentric loading test of RC columns with normal- and high-strength materials and averaged stress–strain model for confined concrete considering compressive fracture energy. In: Proceedings of the 2nd fib Congress, Naples, Italy, 5–8 June 2006, on CD-ROM, ID 3-13
54. Eligehausen R, Popov E, Bertero V (1983) Local bond stress–slip relationship of deformed bars under generalized excitations. Report no. UCB/EERC-83/23, University of California, Berkeley
55. Jenq YS, Shah SP (1989) Shear resistance of reinforced concrete beams—a fracture mechanics approach. In: Li VC, Bazant ZP (eds) Fracture mechanics: application to concrete (special report ACI SP-118). American Concrete Institute, Detroit, pp 327–358
56. Bigaj AJ (1995) Bond behaviour of deformed bars in NSC and HSC—experimental study. Progress in concrete research. Delft Univ Technol 4:91–106
57. Cairns J, Jones K (1995) The splitting forces generated by bond. Mag Concr Res 47:153–165
58. Carpinteri A, Ferro G, Ventura G (2004) Double brittle-to-ductile transition in bending of fibre reinforced concrete beams with rebars. Int J Numer Anal Methods Geomech 28:737–756. doi:10.1002/nag.372
59. Eligehausen R, Fabritius E, Li L, Zhao R (1993) An analysis of rotation capacity tests. CEB Bulletin d'Information 218:251–273